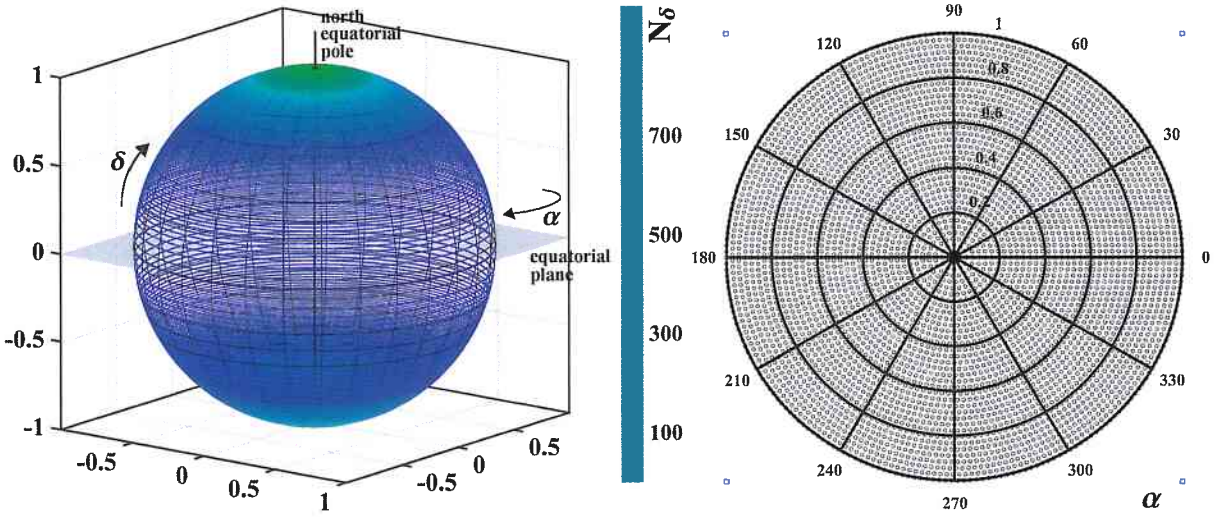

FIG. 1. Tilling of sky-grid for the frequency band 1240-1250 Hz; $d_{\rm sky} = 6.6 \times 10^{-4}$ for this band. In the left panel, we show the sky-grid points on the celestial sphere; the color-code traces the number of sky-grid points, N_δ, as a function of equatorial latitude δ. The right panel is a polar plot of the northern equatorial hemisphere of the same sky-grid but with density scaled down by a factor of 4 to allow for better viewing. In the polar plot, $\theta = \alpha$ and $r = \mathrm{Cos}(\delta)$.

In these regions, depending on the signal parameters, the detection efficiency might be affected.

Quantity	Value
$T_{\rm coh}$ (hours)	30.0
$T_{\rm obs}$ (days)	653.18
$T_{\rm ref}$ (GPS seconds)	847063082.5
$N_{\rm seg}$	205
$\delta f_{\rm c}$ (Hz)	6.71×10^{-6}
$\delta \dot{f}_{\rm c}$ (Hz/s)	5.78×10^{-10}
γ	1399
$m_{\rm sky}$	0.30

TABLE I. Search parameters for the search. $T_{\rm ref}$ is the reference time that defines the frequency and spin-down values.

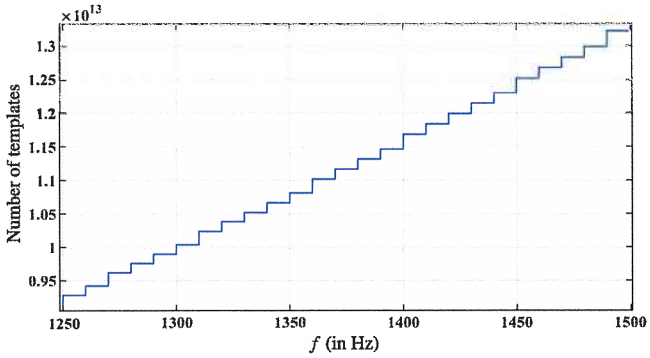

FIG. 2. Number of templates searched in 50 mHz bands. The variation in template count arises from the variation is number of sky-grid points every 10 Hz in frequency. Each 50 mHz band contributes roughly 6.3×10^7 templates in frequency and spin-down (on the finer grid refined by refinement factor γ.)

Despite
In spite of the removal of known disturbances in the data, the data still contains unknown noise artefacts that produce $2\overline{\mathcal{F}}$ values that do not follow the expected distribution for Gaussian noise. These artefacts usually have narrow-band characteristics; we identify such "disturbed" signal-frequency intervals in the search results and exclude them from further consideration. The benefit of such exclusions is that, in the remaining "undisturbed" bands, we can rely on semi-analytic predictions for the significance of the observed $2\overline{\mathcal{F}}$ values, and we can set a uniform detection criteria across the entire parameter space. It is true that we forego the probability of detecting a signal in the disturbed frequency intervals. However, in order to perform reliable analyses in these intervals, ad-hoc studies and tuning of the procedures would need to be performed on each disturbed band separately and these would be very time-consuming. Since the undisturbed intervals in data comprise over 95% of the total data, we believe that ignoring the disturbed bands for this search is a reasonable choice. In the future, a focused effort on the analysis of the disturbed bands could attempt to recover some sensitivity in those regions.

The identification of undisturbed bands is carried out via a *visual inspection method*. This visual inspection of the data is performed by two scientists for this search who look at various distributions of the $2\overline{\mathcal{F}}$ values in $(f, \dot{f})$ parameter space in 50 mHz bands. They rank these 50 mHz bands with 4 numbers: 0,1,2,3; a '0' ranking marks the band as "undisturbed", a '3' ranks the band

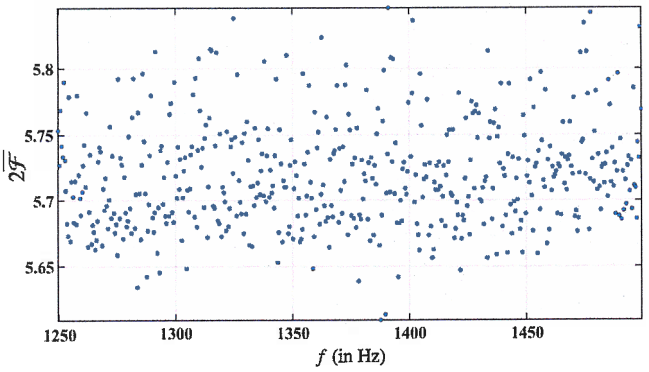

FIG. 4. Highest values of $2\overline{\mathcal{F}}$ in every 0.5 Hz band as a function of starting frequency of the band.

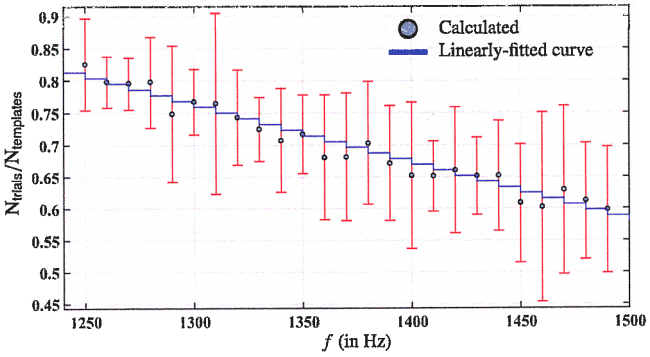

FIG. 5. Ratio $\mathcal{R} = N_{\rm trials}/N_{\rm templates}$ as a function of frequency in 10 Hz intervals. The error bars represent the 1-σ statistical errors from the fitting procedure described in the text, not the linear fit used to draw the blue line shown here.

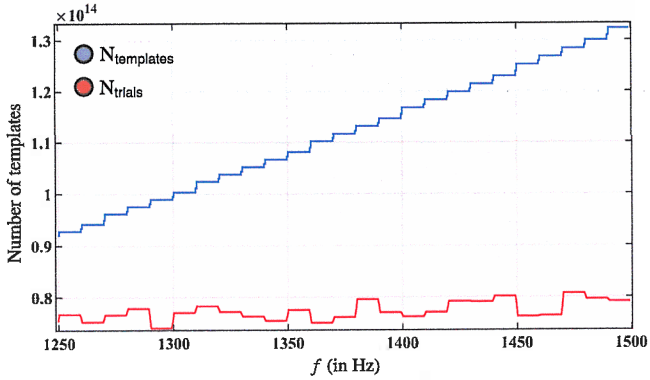

FIG. 6. Values of $N_{\rm templates}$ and $N_{\rm trials}$ as a function of frequency in 0.5 Hz bands.

candidates in 0.5 Hz bands as a function of frequency (top panel) and their distribution (bottom panel).

In this search, the overall loudest candidate with $2\overline{\mathcal{F}} = 5.846$ is also the most significant candidate, with CR = 3.25. A deviation of 3.25σ from expected $2\overline{\mathcal{F}}$ value would not be significant enough to claim a detection if we had only searched a single 0.5 Hz band; in fact, it is even less significant considering the fact that a total of 485 0.5 Hz bands were searched.

We define the p-value associated with a CR as the probability of observing that particular value of CR or higher by random chance in a search over one 0.5 Hz band, performed over $N_{\rm trials}$ number of independent trials using $N_{\rm seg}$ number of segments. The distribution of p-values associated with the loudest observed candidates in 0.5 Hz bands is consistent with what we expect from noise-only scenario across the explored parameter space, as shown in Fig. 9. In particular, note that the loudest observed candidate with CR = 3.25 is consistent with expectations from noise-only scenario, and in fact, there is no population of candidates with low CR values deviating from the expectations from noise-only case. Furthermore, we see in Fig. 9 that across 485 0.5 Hz bands searched by our set up, we expect 4 ± 3 candidates at least as significant as CR = 3.25 by random chance, which makes our observed loudest candidate completely consistent with expectations from noise-only case.

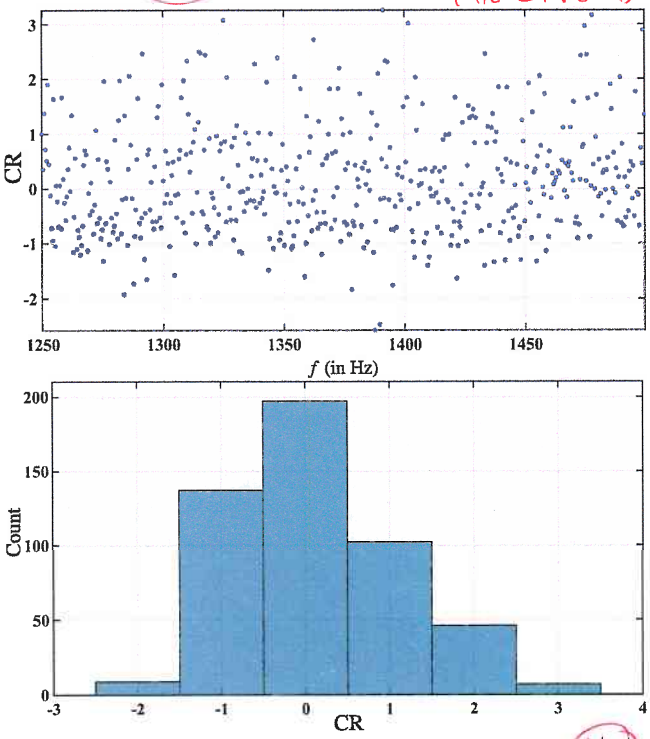

FIG. 7. In the top panel, we plot the significance of loudest observed candidate in every 0.5 Hz band as a function of starting frequency of the band. In the bottom panel, we show the distribution of CR values. The significance folds in the expected value for the loudest $2\overline{\mathcal{F}}$ and its standard deviation.

V. UPPER-LIMITS

Our search results do not deviate from the expectations from noise-only data. Hence, we set frequentist upper-limits on the maximum gravitational wave amplitude, $h_0^{90\%}$, from the target source population consistent

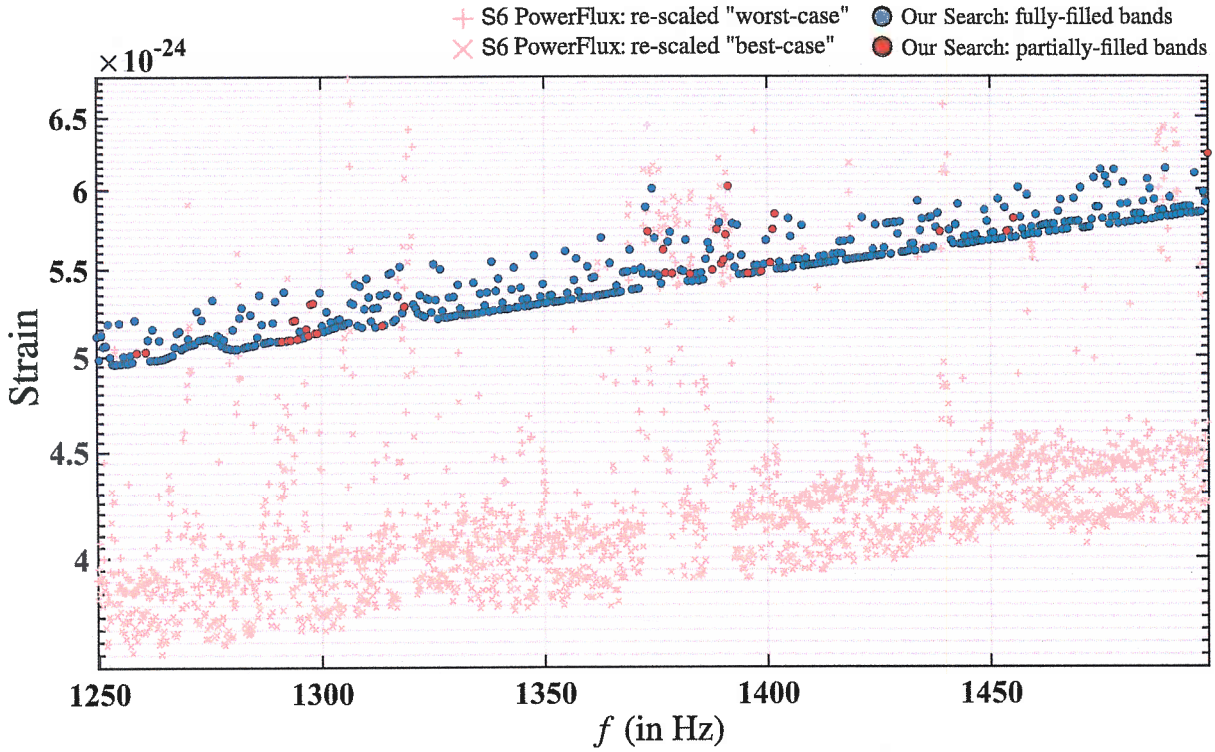

FIG. 10. 90%-confidence upper-limits on the gravitational wave amplitude for signals with frequency within 0.5 Hz bands, over the entire sky, and within the spin-down range of the search described in section III. The red circular markers denote 0.5 Hz bands where the upper-limit value does not hold for all frequencies in that interval; the list of corresponding excluded frequencies is given in Table IV. For reference, we also plot the upper-limit results from the only other high-frequency search [10], on significantly more sensitive S6 data. It should be noted that the *PowerFlux* upper-limits are set at 95%-confidence rather than 90%-confidence level as in this search, but also refer to 0.25 Hz bands rather than 0.5 Hz bands.

the S6 run data is about a factor 2.4 more sensitive compared to the S5 data used in this search. We can express the $h_0^{90\%}$ upper-limits as bounds on the maximum distance from Earth within which we can exclude a rotating compact object emitting continuous gravitational waves at a given frequency f due to a fixed and non-axisymmetric mass quadrupole moment, characterised by ϵI, with I being the principal moment of inertia, and ϵ the ellipticity of the object. The GW-spindown is the fraction of spin-down, $x|\dot{f}|$, responsible for continuous gravitational wave emission [12]. The ellipticity ϵ of the compact object necessary to sustain such emission is then given by,

$$\epsilon(f, x|\dot{f}|) = \sqrt{\frac{5c^5}{32\pi^4 G}\frac{x|\dot{f}|}{If^5}}, \tag{5}$$

where, c is the speed of light, G is the Gravitational constant. Moreover, since the gravitational wave amplitude for an object at a distance d, with an ellipticity ϵ given by (5), is expressed as

$$h_0(f, x|\dot{f}|, d) = \frac{1}{d}\sqrt{\frac{5IG}{2c^3}\frac{x|\dot{f}|}{f}}, \tag{6}$$

we can recast the $h_0^{90\%}$ upper-limit curves as $(f, x|\dot{f}|)$ curves parametrised by different values of the distance d, as shown in Fig.11. We also show the contours of constant ellipticity for reference. We find that within 100 pc of Earth, our upper-limits exclude objects with ellipticities higher than roughly $2.8 \times 10^{-7}\left[\frac{10^{38}\text{kg m}^2}{I}\right]$, corresponding to GW-spindown values between roughly 4.0×10^{-10} and 1.0×10^{-9} Hz/s.

The search presented here is probably the last all-sky search on S5 data, and by inspecting the higher frequency range for continuous gravitational wave emission, it concludes the Einstein@Home observing campaign on this data. Consistent with the recent results on S6 data [10], we also find no continuous GW signal in the S5 data. However, mechanisms for transient or intermittent GW emission have been proposed [15, 16] that would not a priori exclude a signal during S5 run but not during S6 run; this makes the search presented here meaningful.

VII. ACKNOWLEDGMENTS

Maria Alessandra Papa gratefully acknowledges the support from NSF PHY Grant 1104902. All the

post-processing computational work for this search was carried out on ATLAS super-computing cluster at the Max-Planck-Institut für Gravitationsphysik/ Leibniz Universität Hannover. We also acknowledge the Continuous Wave Group within LIGO Scientific Collaboration, the LIGO Scientific Collaboration, and the reviewers in the Presentations & Publications committee of LIGO Scientific Collaboration for providing us with valuable feedback.

* * *

Appendix A: Tabular data

1. Upper-limit $h_0^{90\%}$ values

f (in Hz)	$h_0^{90\%} \times 10^{24}$	f (in Hz)	$h_0^{90\%} \times 10^{24}$	f (in Hz)	$h_0^{90\%} \times 10^{24}$	f (in Hz)	$h_0^{90\%} \times 10^{24}$
1249.717	5.1 ± 1.0	1250.217	5.0 ± 0.9	1250.717	5.1 ± 1.0	1251.217	5.1 ± 0.9
1251.717	5.1 ± 0.9	1252.217	5.2 ± 1.0	1252.717	5.0 ± 0.9	1253.217	5.0 ± 0.9
1253.717	5.0 ± 0.9	1254.217	5.0 ± 0.9	1254.717	5.2 ± 1.0	1255.217	5.0 ± 0.9
1255.717	5.0 ± 0.9	1256.217	5.0 ± 0.9	1256.717	5.0 ± 0.9	1257.217	5.0 ± 0.9
1257.717	5.0 ± 0.9	1258.217	5.2 ± 1.0	1258.717	5.0 ± 0.9	1260.717	5.0 ± 0.9
1261.217	5.1 ± 0.9	1261.717	5.0 ± 0.9	1262.217	5.2 ± 1.0	1262.717	5.0 ± 0.9
1263.217	5.0 ± 0.9	1263.717	5.1 ± 0.9	1264.217	5.0 ± 0.9	1264.717	5.0 ± 0.9
1265.217	5.0 ± 0.9	1265.717	5.0 ± 0.9	1266.217	5.0 ± 0.9	1266.717	5.0 ± 0.9
1267.217	5.1 ± 1.0	1267.717	5.1 ± 0.9	1268.217	5.1 ± 0.9	1268.717	5.0 ± 0.9
1269.217	5.1 ± 0.9	1269.717	5.1 ± 0.9	1270.217	5.1 ± 1.0	1270.717	5.1 ± 0.9
1271.217	5.1 ± 0.9	1271.717	5.1 ± 0.9	1272.217	5.3 ± 1.0	1272.717	5.1 ± 0.9
1273.217	5.2 ± 1.0	1273.717	5.1 ± 0.9	1274.217	5.1 ± 0.9	1274.717	5.1 ± 0.9
1275.217	5.1 ± 0.9	1275.717	5.3 ± 1.0	1276.217	5.1 ± 0.9	1276.717	5.1 ± 1.0
1277.217	5.1 ± 1.0	1277.717	5.1 ± 0.9	1278.217	5.1 ± 1.0	1278.717	5.0 ± 0.9
1279.217	5.0 ± 0.9	1279.717	5.0 ± 0.9	1280.217	5.2 ± 0.9	1280.717	5.0 ± 0.9
1281.217	5.0 ± 0.9	1281.717	5.2 ± 1.0	1282.217	5.3 ± 1.0	1282.717	5.0 ± 0.9
1283.217	5.1 ± 0.9	1283.717	5.1 ± 0.9	1284.217	5.2 ± 1.0	1284.717	5.1 ± 0.9
1285.217	5.1 ± 0.9	1285.717	5.1 ± 1.0	1286.217	5.3 ± 1.1	1286.717	5.2 ± 1.0
1287.217	5.1 ± 0.9	1287.717	5.1 ± 0.9	1288.217	5.1 ± 0.9	1288.717	5.1 ± 0.9
1289.217	5.2 ± 1.0	1289.717	5.3 ± 1.0	1290.217	5.1 ± 0.9	1290.717	5.1 ± 0.9
1291.217	5.1 ± 0.9	1291.717	5.4 ± 1.1	1292.217	5.1 ± 0.9	1292.717	5.1 ± 0.9
1293.217	5.1 ± 0.9	1293.717	5.2 ± 1.0	1294.217	5.2 ± 1.0	1294.717	5.1 ± 0.9
1295.217	5.1 ± 1.0	1295.717	5.1 ± 0.9	1296.217	5.1 ± 0.9	1296.717	5.2 ± 1.0
1297.217	5.1 ± 0.9	1297.717	5.3 ± 1.0	1298.217	5.3 ± 1.0	1298.717	5.1 ± 0.9
1299.217	5.1 ± 0.9	1299.717	5.4 ± 1.0	1300.217	5.2 ± 1.0	1300.717	5.1 ± 0.9
1301.217	5.3 ± 1.0	1301.717	5.1 ± 0.9	1302.217	5.2 ± 1.0	1302.717	5.2 ± 0.9
1303.217	5.2 ± 0.9	1303.717	5.2 ± 1.0	1304.217	5.2 ± 1.0	1304.717	5.2 ± 0.9

f (in Hz)	$h_0^{90\%} \times 10^{24}$	f (in Hz)	$h_0^{90\%} \times 10^{24}$	f (in Hz)	$h_0^{90\%} \times 10^{24}$	f (in Hz)	$h_0^{90\%} \times 10^{24}$
1407.217	5.6 ± 1.0	1407.717	5.8 ± 1.1	1408.217	5.5 ± 1.0	1408.717	5.6 ± 1.0
1409.217	5.5 ± 1.0	1409.717	5.5 ± 1.0	1410.217	5.5 ± 1.0	1410.717	5.5 ± 1.0
1411.217	5.5 ± 1.0	1411.717	5.6 ± 1.0	1412.217	5.5 ± 1.0	1412.717	5.6 ± 1.0
1413.217	5.5 ± 1.0	1413.717	5.5 ± 1.0	1414.217	5.5 ± 1.0	1414.717	5.6 ± 1.1
1415.217	5.5 ± 1.0	1415.717	5.6 ± 1.1	1416.217	5.7 ± 1.0	1416.717	5.6 ± 1.1
1417.217	5.7 ± 1.0	1417.717	5.6 ± 1.0	1418.217	5.6 ± 1.0	1418.717	5.7 ± 1.0
1419.217	5.6 ± 1.0	1419.717	5.6 ± 1.0	1420.217	5.6 ± 1.0	1420.717	5.6 ± 1.0
1421.217	5.8 ± 1.1	1421.717	5.6 ± 1.0	1422.217	5.6 ± 1.0	1422.717	5.6 ± 1.0
1423.217	5.6 ± 1.0	1423.717	5.6 ± 1.1	1424.217	5.8 ± 1.1	1424.717	5.6 ± 1.0
1425.217	5.6 ± 1.0	1425.717	5.6 ± 1.0	1426.217	5.6 ± 1.1	1426.717	5.8 ± 1.1
1427.217	5.8 ± 1.1	1427.717	5.6 ± 1.0	1428.217	5.8 ± 1.1	1428.717	5.8 ± 1.1
1429.217	5.7 ± 1.1	1429.717	5.8 ± 1.1	1430.217	5.6 ± 1.0	1430.717	5.6 ± 1.0
1431.217	5.6 ± 1.0	1431.717	5.6 ± 1.0	1432.217	5.6 ± 1.1	1432.717	5.7 ± 1.1
1433.217	5.6 ± 1.0	1433.717	5.9 ± 1.2	1434.217	5.7 ± 1.1	1434.717	5.8 ± 1.1
1435.217	5.6 ± 1.0	1435.717	5.6 ± 1.0	1436.217	5.8 ± 1.1	1436.717	5.8 ± 1.1
1437.217	5.6 ± 1.0	1437.717	5.8 ± 1.1	1438.217	5.8 ± 1.1	1438.717	5.7 ± 1.1
1440.717	5.7 ± 1.1	1441.217	5.7 ± 1.0	1441.717	5.7 ± 1.0	1442.217	5.8 ± 1.1
1442.717	5.9 ± 1.1	1443.217	5.6 ± 1.0	1443.717	5.6 ± 1.0	1444.217	5.7 ± 1.1
1444.717	5.7 ± 1.0	1445.217	5.7 ± 1.0	1445.717	5.7 ± 1.1	1446.217	5.7 ± 1.0
1446.717	5.7 ± 1.1	1447.217	5.7 ± 1.0	1447.717	5.7 ± 1.0	1448.217	5.7 ± 1.0
1448.717	5.9 ± 1.1	1449.217	5.8 ± 1.1	1449.717	5.7 ± 1.0	1450.217	5.7 ± 1.1
1450.717	5.7 ± 1.1	1451.217	5.7 ± 1.0	1451.717	5.9 ± 1.1	1452.217	5.7 ± 1.0
1452.717	5.7 ± 1.0	1453.217	5.9 ± 1.1	1453.717	5.7 ± 1.1	1454.217	5.7 ± 1.1
1454.717	5.7 ± 1.0	1455.217	5.8 ± 1.1	1455.717	5.7 ± 1.0	1456.217	6.0 ± 1.2
1456.717	5.8 ± 1.1	1457.217	5.7 ± 1.1	1457.717	5.7 ± 1.0	1458.217	6.0 ± 1.1
1458.717	5.7 ± 1.0	1459.217	5.8 ± 1.1	1459.717	5.7 ± 1.0	1460.217	5.8 ± 1.1
1460.717	5.7 ± 1.0	1461.217	5.8 ± 1.1	1461.717	5.8 ± 1.1	1462.217	5.8 ± 1.1
1462.717	5.8 ± 1.1	1463.217	5.7 ± 1.0	1463.717	5.8 ± 1.1	1464.217	5.8 ± 1.1
1464.717	5.7 ± 1.0	1465.217	5.9 ± 1.1	1465.717	5.9 ± 1.1	1466.217	5.7 ± 1.0
1466.717	5.8 ± 1.1	1467.217	5.7 ± 1.0	1467.717	5.8 ± 1.1	1468.217	5.8 ± 1.1
1468.717	5.9 ± 1.2	1469.217	5.8 ± 1.1	1469.717	5.8 ± 1.1	1470.217	6.0 ± 1.2
1470.717	5.7 ± 1.0	1471.217	5.7 ± 1.0	1471.717	5.8 ± 1.0	1472.217	5.8 ± 1.0
1472.717	5.8 ± 1.1	1473.217	6.1 ± 1.2	1473.717	5.9 ± 1.1	1474.217	5.9 ± 1.1
1474.717	6.1 ± 1.3	1475.217	5.8 ± 1.1	1475.717	6.1 ± 1.2	1476.217	6.0 ± 1.2
1476.717	5.8 ± 1.0	1477.217	5.8 ± 1.1	1477.717	6.1 ± 1.1	1478.217	5.8 ± 1.1
1478.717	5.8 ± 1.0	1479.217	5.9 ± 1.1	1479.717	6.0 ± 1.2	1480.217	5.8 ± 1.0
1480.717	5.9 ± 1.1	1481.217	5.8 ± 1.0	1481.717	5.8 ± 1.0	1482.217	5.8 ± 1.1
1482.717	5.8 ± 1.1	1483.217	5.8 ± 1.0	1483.717	5.8 ± 1.1	1484.217	5.9 ± 1.1
1484.717	5.8 ± 1.0	1485.217	6.1 ± 1.2	1485.717	6.0 ± 1.2	1486.217	5.8 ± 1.0
1486.717	5.9 ± 1.1	1487.217	5.8 ± 1.0	1487.717	5.9 ± 1.1	1488.217	5.8 ± 1.0
1488.717	5.9 ± 1.1	1489.217	6.1 ± 1.2	1489.717	5.8 ± 1.0	1490.217	5.9 ± 1.1
1490.717	5.8 ± 1.0	1491.217	5.9 ± 1.1	1491.717	5.8 ± 1.0	1492.217	5.9 ± 1.1
1492.717	5.8 ± 1.0	1493.217	5.9 ± 1.1	1493.717	5.9 ± 1.1	1494.217	5.8 ± 1.0
1494.717	5.9 ± 1.1	1495.217	5.8 ± 1.0	1495.717	6.1 ± 1.2	1496.217	5.8 ± 1.0
1496.717	5.8 ± 1.0	1497.217	5.9 ± 1.0	1497.717	6.0 ± 1.1	1498.217	5.9 ± 1.1
1498.717	6.3 ± 1.3	–	–	–	–	–	–

TABLE II. Left column denotes the starting frequency of each 0.5-Hz signal-frequency band in which we set upper-limits; right column states the upper-limit value i.e. $h_0^{90\%}$, for that 0.5 Hz band. Note: the $h_0^{90\%}$ values quoted here include additional 10% uncertainty introduced by data calibration procedure.

4. Omitted 50 Hz bands from Signal-frequency

f_{start} (in Hz)	f_{end} (in Hz)	Type	f_{start} (in Hz)	f_{end} (in Hz)	Type
1258.617	1258.717	D	1259.217	1260.767	C
1291.017	1291.067	D	1292.567	1292.867	D
1293.267	1293.567	D	1293.917	1294.217	D
1296.367	1296.817	D	1297.517	1297.717	D
1298.667	1298.967	D	1313.467	1313.517	D
1318.567	1318.667	D	1319.217	1320.767	C
1372.867	1373.167	D	1376.417	1376.817	D
1378.517	1378.617	D	1379.217	1380.767	C
1382.567	–	D	1387.317	–	D
1387.767	1388.217	D	1388.417	1388.567	C
1389.467	–	D	1389.767	1390.217	D
1390.467	1390.867	D	1390.967	1391.117	D
1395.217	1395.467	D	1398.417	1398.667	D
1399.967	1400.867	D	1400.967	1401.267	D
1438.417	1438.517	D	1439.217	1440.767	C
1453.467	1453.517	D	1454.967	1455.067	D
1498.317	1498.467	D	1499.267	1499.417	C

TABLE V. 50-mHz search-frequency bands that were identified as "disturbed" based on Visual Inspection (D), or where the results were produced from "All Fake Data" as detailed in table IV (C). Both sets of bands (D and C) were excluded from the analysis. The first two columns list the starting frequency of the first and last 50-mHz band in the contiguous range of excluded bands.

[1] J Aasi *et al* (LIGO Scientific Collaboration). *Directed search for continuous gravitational waves from the Galactic center*. **Phys. Rev. D**, 88(10):102002, 2013.

[2] J Aasi *et al* (LIGO Scientific Collaboration). *Einstein@Home all-sky search for periodic gravitational waves in LIGO S5 data*. **Phys. Rev. D**, 87(8):042001, 2013.

[3] J Abadie *et al* (LIGO Scientific Collaboration). *Calibration of the LIGO gravitational wave detectors in the fifth science run*. **Nucl. Instrum. Meth. A**, 624(1):223–240, 2010.

[4] B Abbot *et al* (LIGO Scientific Collaboration). *Searches for periodic gravitational waves from unknown isolated sources and Scorpius X-1: Results from the second LIGO science run*. **Phys. Rev. D**, 76(8):082001, 2007.

[5] B Abbot *et al* (LIGO Scientific Collaboration). *All-sky search for periodic gravitational waves in LIGO S4 data*. **Phys. Rev. D**, 77(2):022001, 2008.

[6] B Abbot *et al* (LIGO Scientific Collaboration). *LIGO: the Laser Interferometer Gravitational-Wave Observatory*. **Rep. Prog. Phys.**, 72(7):076901, 2009.

[7] B Abbot *et al* (LIGO Scientific Collaboration). *All-Sky LIGO Search for Periodic Gravitational Waves in the Early Fifth-Science-Run Data*. **Phys. Rev. Lett.**, 102 (11):111102, 2009.

[8] B Abbot *et al* (LIGO Scientific Collaboration). *All-sky search for periodic gravitational waves in the full S5 LIGO data*. **Phys. Rev. D**, 85(2):022001, 2012.

[9] B Abbot *et al* (LIGO Scientific Collaboration). *Results of an all-sky Einstein@Home search for continuous gravitational waves*. **Phys. Rev. D**, –(–):–, 2016. submitted; arXiv:xxxx:xxxxx.

[10] B Abbot *et al* (LIGO Scientific Collaboration). *Comprehensive All-sky Search for Periodic Gravitational Waves in the Sixth Science Run LIGO Data*. **arXiv:1605.03233**, 2016.

[11] C Cutler and B F Schutz. *Generalized $\mathcal{F}$-statistic: Multiple detectors and multiple gravitational wave pulsars*. **Phys. Rev. D**, 72(6):063006, 2005.

[12] J Ming *et al*. *Optimal directed searches for continuous gravitational waves*. **Phys. Rev. D**, 93(6):064011, 2016.

[13] H J Pletsch. *Parameter-space correlations of the optimal statistic for continuous gravitational-wave detection*. **Phys. Rev. D**, 78(10):102005, 2008.

[14] H J Pletsch. *Parameter-space metric of semicoherent searches for continuous gravitational waves*. **Phys. Rev. D**, 82(4):042002, 2010.

[15] R Prix, S Giampanis, and C Messenger. *Search method for long-duration gravitational-wave transients from neutron stars*. **Phys. Rev. D**, 84(2):023007, 2011.

[16] A Singh. *Gravitational Wave transient signal emission via Ekman Pumping in Neutron Stars during post-glitch relaxation phase*. **Phys. Rev. D**, –(–):–, 2016. submitted; arXiv:1605.08420.

[17] K Wette. *Estimating the sensitivity of wide-parameter-space searches for gravitational-wave pulsars*. **Phys. Rev. D**, 85(4):042003, 2012.